# Exploration of Orange Peel Waste as Precursor for the Synthesis and Characterization of highly Crystalline and Mesoporous Silicon Oxide Nanoparticles

**Richard Alexis Ukpe and Heleen Chima Anyalechi**

**Abstract:** *This study presents a sustainable and eco-friendly approach to synthesizing silicon oxide nanoparticles (SiONPs) using orange peel waste as a precursor. The research aims to investigate the presence and suitability of biomolecules within orange peel waste for reducing silicon precursors into SiONPs, optimize the synthesis process, characterize the synthesized nanoparticles, explore potential applications, and address knowledge gaps in utilizing waste materials for SiONP synthesis. The significance of the study lies in its contributions to sustainability, environmental friendliness, cost-effectiveness, and novel application of orange peel waste. By utilizing green synthesis methods, the study reduces environmental impact, promotes circular economy principles, and introduces a cost-effective alternative for SiONP production. Additionally, the study fills a critical knowledge gap by being the first to directly utilize orange peel waste for SiONP synthesis, potentially revolutionizing SiONP production and promoting a greener future. The scope involves exploring biomolecules in orange peel waste, optimizing synthesis processes, characterizing SiONPs, and exploring initial applications. While the study focuses on orange peel waste, its findings may have broader implications for utilizing other citrus fruit peels or plant waste in nanoparticle synthesis. Limitations include the focus on specific waste, limited exploration of applications, scalability challenges, and the need for long-term stability assessments. Research questions guide the study, addressing the presence of silicon-containing biomolecules in orange peel waste, optimal synthesis conditions, characteristics of synthesized SiONPs, and preliminary functionalities for potential applications. Overall, this research contributes to advancing sustainable nanotechnology practices and offers promising avenues for waste utilization and nanoparticle synthesis.*

**Richard Alexis Ukpe**
Federal University, Otuoke,
Bayelsa State, Nigeria
**Email: ukpera@fuotuoke.edu.ng**
**Orcid id: 0000-0002-1010-4433**

**Heleen Chima Anyalechi**
Department of Pure and Industrial Chemistry, University of Nigeria, Nsukka, Enugu State.

## 1.0    Introduction

The expansion of the field of nanotechnology is due to the high demand but limited supply of nanoparticles especially, the eco-friendly nanoproducts (Anjum *et al*., 2023). However, the traditional synthesis methods often rely on harsh chemicals and high-energy consumption. This raises environmental and health concerns. Green synthesis, which utilizes plant extracts for nanoparticle formation, offers a sustainable and eco-friendly alternative. Plant waste, a readily available and renewable resource, plays a crucial role in this process. Various plant parts, including leaves, stems, roots, and even fruits, harbour a wealth of biomolecules like alkaloids, terpenoids, and phenolics (Rashwan *et al*., 2023). These biomolecules act as both

reducing and capping agents, facilitating the reduction of metal ions into nanoparticles and preventing their aggregation (Bishnoi *et al.*, 2018).

Green synthesis offers numerous advantages over conventional methods. It eliminates the need for toxic chemicals, minimizing environmental impact and worker exposure (Omran, 2020). Additionally, plant extracts can be readily obtained, making the process cost-effective (Tavker *et al.*, 2021). Furthermore, nanoparticles synthesized using plant extracts often exhibit unique properties, such as enhanced biocompatibility and controlled release of substances (Garg *et al.*, 2021, 2022). The green synthesis process typically involves extracting bioactive compounds from plant material and using them to reduce metal salts in solution. The resulting nanoparticles can be characterized using various techniques like UV-Vis spectroscopy, X-ray diffraction (XRD), and Fourier-transform infrared spectroscopy (FTIR) to determine their size, shape, and composition (More *et al.*, 2023; Eddy *et al.*, 2023i).

Plant-based nanoparticles have diverse applications across various sectors. In the environmental realm, they can be employed for wastewater treatment due to their efficient adsorption capabilities (Ying *et al.*, 2022). In biomedicine, they hold promise for drug delivery, targeted therapy, and anti-microbial applications (Kazemi *et al.*, 2023). Moreover, they can be used in agriculture to enhance crop yield and combat plant diseases (Khan *et al.*, 2019).

Despite the significant advancements, challenges remain. Refining the synthesis process to achieve precise control over nanoparticle size and morphology is crucial. Additionally, ensuring the scalability of green synthesis for large-scale production is essential (Xu *et al.*, 2019).

The utilization of plant waste for nanoparticle synthesis presents a sustainable and eco-friendly approach. With ongoing research to optimize the process and address existing challenges, this approach has the potential to revolutionize various fields, promoting a greener future for nanotechnology.

Also, the ever-growing utilization of edible plant materials has created competition in the food sector and the possibility of a food security-based attack is most likely if the current trend is not properly arrested. In this quest, agricultural waste materials have emerged as promising candidates due to their abundance, low cost, and inherent biocompatibility. Among these, orange peel, a significant by-product of the citrus industry, presents a compelling opportunity for the synthesis of various nanoparticles. Citrus fruits, particularly oranges, are a major agricultural crop cultivated worldwide. This cultivation generates a substantial amount of orange peel waste, estimated to be around 60-70% of the total fruit weight (Eddy *et al.*, 2023a). Traditionally, orange peel waste poses a disposal challenge, often ending up in landfills or undergoing inefficient composting processes. Utilizing orange peel waste for nanoparticle synthesis offers a sustainable solution by converting a waste product into a valuable resource.

Orange peel is a rich source of various biomolecules that play a crucial role in nanoparticle synthesis. These biomolecules including cellulose and hemicellulose, lignin, pectins, bioactive compounds such as flavonoids, terpenoids, and organic acids (Eddy *et al.*, 2023). These set of compounds have the advantages of facilitating the reduction of metal salt to AgNPs (Mostafa *et al.*, 2021; Skiba, 2019), ZnONPs (Doan Thi *et al.*, 2020), SeNPs (Dang-Bao *et al.*, 2022; Salem *et al.*, 2022), TiONPs (Amanulla *et al.*, 2019), FeONPs (Bashir *et al.*, 2020). However, no report on the direct application of orange peel waste as a precursor for the synthesis of nanoparticles has been documented. Some literature has shown that plants, including citrus fruits, are known to absorb silicon from

the soil (Epstein, 1999). Silicon plays a vital role in plant cell wall strength and various physiological processes (Ma & Takahashi, 2002). However, the specific amount in orange peels remains unclear, the presence of silicon is highly probable due to its role in plant health. The present study seeks to investigate the possibility of synthesizing silicon oxide nanoparticles using orange peel waste as the precursor.

## 2.0　Materials and Methods
### 2.1　Sample collection
Samples of fresh oranges were purchased from a market within the University of Nigeria, Nsukka. The peels were carefully removed from the edible portion, and dried to constant weight before they were grounded to a powdered form

### 2.2　Synthesis of Silicon Nanoparticles:
200 g of dried and ground orange sample was weighed and poured into a clean, dry bowl. 200 ml of the diluted HCl solution was gradually added to the dried sugarcane sample, ensuring thorough mixing using a stirring rod until no gas was evolved. The reaction equation is as follows:

$$Si_{(s)} + 2HCl_{(s)} \rightarrow SiCl_{(aq)} + H_{2(G)}$$
$$(1)$$
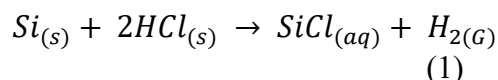
Next, the prepared NaOH solution was added to the reaction mixture containing orange peel and hydrochloric acid (HCl), and mixed gently and thoroughly. The reaction vessel was covered and left overnight to allow the mixture to react and form a gel. The reaction equation is as follows,

$$SiCl_{2(aq)} + NaOH_{(aq)} \rightarrow$$
$$Si(OH)_2 \ 2NaCl_{(aq)} + H_2O_{(l)}$$
$$(2)$$
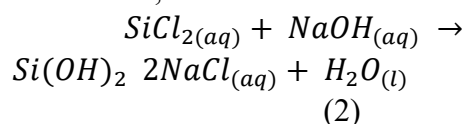
b. Filtration, Drying, and Calcination: The gel was filtered using a sieve to separate the solid residue (chaff) from the liquid phase. The treated residue was washed several times with distilled water and sieved to remove soluble sodium chloride. The residue (nanoparticles) was collected and dried in an oven at 105°C to remove residual moisture. The dried residue weighed 67.025 g. Subsequently, 19.742 g of the residue was placed in a crucible and calcinated in a furnace for 2 hours and 30 minutes at 800°C in a controlled environment to induce further chemical changes. After calcination, the ash (nanoparticles) was allowed to cool and collected in a clean sample container for characterization.

### 2.3　Characterization of Nanoparticles
### 2.3.1　UV Visible Analysis
The methodology for analyzing the wavelength and bandgap of nanoparticles using a Shimadzu UV-visible spectrophotometer was conducted as follows:

i. **Sample Preparation**: Nanoparticles were prepared in a suitable solvent to create a clear solution, ensuring that the concentration was within the optimal range for absorbance measurements.

ii. **Instrument Calibration**: The spectrophotometer was calibrated with a blank solvent to establish a baseline for zero absorbance at all wavelengths of interest.

iii. **Parameter Settings**: The analysis parameters, including the wavelength range and the scan rate, were set on the spectrophotometer. The wavelength range was chosen to cover the expected bandgap energies of the nanoparticles.

iv. **Loading the Sample**: The nanoparticle solution was transferred into a quartz cuvette, which was then placed in the sample holder of the spectrophotometer.

v. **Measurement**: The spectrophotometer scanned the sample across the set wavelength range, measuring the absorbance at each point. The data collected included both the absorbance peaks and the baseline absorbance.

vi. **Data Analysis**: The absorbance spectrum was analyzed to determine the bandgap energy of the nanoparticles. This was done by identifying the

wavelength at which the absorbance began to increase significantly, indicating the onset of electronic transitions related to the bandgap.

vii.   **Reporting Results**: The analyzed data, including the determined bandgap energy and the corresponding wavelength, were documented in a report, along with the full absorbance spectrum.

## 2.3.2   FTIR analysis

FTIR instrument (Agilent infrared spectrophotometer, carrying 630 FTIR spectrometer) was also employed to obtain the infrared absorption of the nanoparticles after scanning through a wave number range of 400 to 4000 cm$^{-1}$. The nanoparticles were directly placed in the sample holder and covered. The wavelength and other selections were set and the data generated were used to plot the graphs.

## 2.3.3   *Crystallinity analysis*

The crystallinity of the synthesized CaO-NP was investigated using XRD Model Nr. ARLXTRA-Xray-XRD through the following steps,

i.   **Sample Preparation**: The nanoparticles were ground into a fine powder to ensure homogeneity and a representative interaction with the X-ray beam.

ii.   **Mounting the Sample**: The powder was evenly distributed onto the sample holder of the XRD instrument, avoiding any preferred orientation.

iii.   **Setting Up the Instrument**: The ARLXTRA X-ray XRD was set up by adjusting the voltage and current of the X-ray tube, selecting the Cu Kα radiation wavelength, and calibrating the detector.

iv.   **Data Collection**: X-rays were directed at the sample, and the diffracted rays were detected over a range of 2θ angles. The intensity of the diffracted X-rays was recorded, creating a diffraction pattern characteristic of the sample's crystalline structure.

v.   **Data Analysis**: The diffraction pattern was analyzed using Bragg's Law:
$$n\lambda = 2d\sin\theta$$
where (n) is the order of reflection, ($\lambda$) is the wavelength of X-rays, ( d ) is the distance between atomic planes in the crystal, and ( $\theta$ ) is the angle of incidence. Peaks in the diffraction pattern corresponded to specific planes within the crystal structure.

vi.   **Interpretation**: The positions and intensities of the peaks were used to identify the phases present in the sample. The analysis provided information on the unit cell dimensions, crystallinity, and phase purity of the nanoparticles.

vii.   **Reporting Results**: The findings were documented in a report, detailing the crystalline phases identified and any structural information obtained from the analysis.

## 2.3.4   *Surface morphology*

The surface morphology and the EDX spectra of the CaO-NP were obtained using a ZEISS EVO scanning electron microscope. The prepared nanoparticle sample was mounted onto SEM stubs using conductive adhesive or double-sided carbon tape. The sample was allowed to dry completely to prevent artefacts during imaging. The instrument was turned on and allowed to warm up. The vacuum levels were adjusted to the recommended settings for high-resolution imaging. The instrument was calibrated to ensure optimal performance, including beam alignment, focus, and astigmatism correction. The accelerating voltage and the beam current were set.

## 3.0   Results and Discussion
## 3.1   *Crystallinity*

The XRD pattern of SiONPs is shown in Fig. 1 while parameters deduced from the plots are provided in Table 1. The results contain useful information concerning the crystalline structure, phase composition, crystallite size, lattice microstrain, and interplanar distance of the SiONiPs.

The XRD peaks correspond to various crystallographic planes of silicon dioxide (SiO2) nanoparticles. Phases identified include Quartz, Tridymite, and Cristobalite, which are common polymorphs of SiO₂. The crystallite size of the various components of the SiONPs was calculated using the Scherrer equation given as equation 4.1 (Eddy *et al*., 2024a-d)

$$d_x = \frac{k\lambda}{\beta cos\theta}$$

(3)

In equation 4.1, $\lambda$ is the wavelength of the Cu-k line, k is the Scherrer constant and $\beta$ is the line broadening. Calculated values of the crystallite size for the various phases are recorded in Table 4.1. The $d_x$ values ranged from 0.741 to 22.15 with an average value of 6.41 nm. The observed values of $d_x$ confirm that the synthesized compound has a nano dimension. The observed values are not out of a comparable range when compared to values obtained from others for SiONPs from plants which are provided in Table 2. The crystallite size ($d_x$) ranges from nanometers to a few tens of nanometers, indicating the size of the crystalline domains within the nanoparticles. Larger crystallite sizes are observed for peaks with lower 2Theta values, indicating larger crystal domains

The lattice microstrain was calculated using equation 4 (Garg *et al*., 2024a-b)
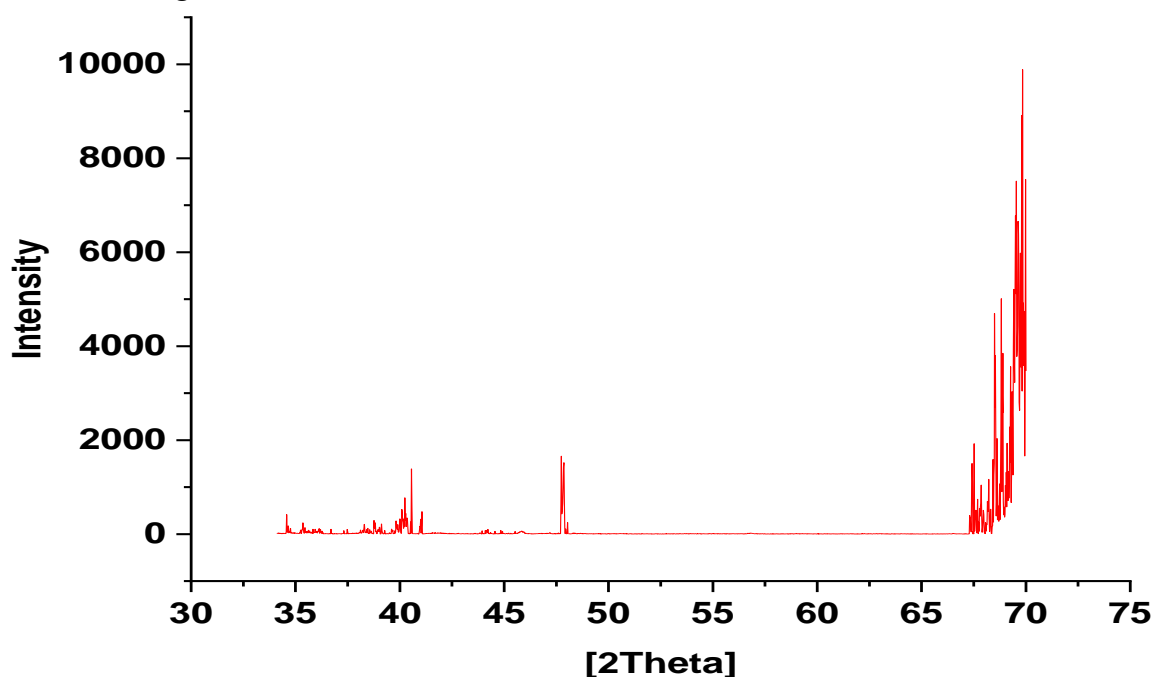
$$\varepsilon = \frac{\beta}{4tan\vartheta}$$

(4)



**Fig. 1: X-ray diffraction pattern of SiONPs synthesized from orange peel**

**Table 1: Crystalline properties of SiONPs obtained from orange peels**

| 2Theta | Phase | (hkl) | SiO2 Phase(s) | $d_x(nm)$ | ε | $d_{(\theta)}$ (Å) |
|--------|-------|-------|---------------|-----------|---|---------------------|
| 39.63 | SiO₂ | -101 | Quartz, Tridymite, Cristobalite | 8.743 | 0.0003 | 1.535 |
| 41.2 | SiO₂ | -110 | Quartz, Tridymite, Cristobalite | 22.115 | 0.0002 | 1.487 |
| 40.95 | SiO₂ | -102 | Quartz, Tridymite, Cristobalite | 9.103 | 0.0003 | 1.503 |
| 41.03 | SiO₂ | -111 | Quartz, Tridymite, Cristobalite | 8.932 | 0.0003 | 1.498 |
| 47.68 | SiO₂ | -200 | Quartz, Tridymite, Cristobalite | 2.167 | 0.0002 | 1.359 |
| 67.35 | SiO₂ | -400 | Quartz, Tridymite, Cristobalite | 2.855 | 0.0083 | 1.563 |
| 69.60717 | SiO₂ | -111 | Quartz, Tridymite, Cristobalite | 3.259 | 0.0047 | 3.134 |
| 69.16262 | SiO₂ | -220 | Quartz | 6.221 | 0.0012 | 2.186 |
| 69.72375 | SiO₂ | -311 | Quartz | 6.778 | 0.0019 | 2.08 |
| 68.66472 | SiO₂ | -200 | Quartz, Tridymite, Cristobalite | 7.813 | 0.0011 | 1.913 |
| 69.75139 | SiO₂ | -222 | Quartz, Tridymite, Cristobalite | 0.742 | 0.1553 | 7.121 |
| 69.75139 | SiO₂ | -222 | Quartz, Tridymite, Cristobalite | 1.025 | 0.0506 | 5.176 |
| 69.75139 | SiO₂ | -222 | Quartz, Tridymite, Cristobalite | 7.7.1 | 0.0003 | 0.68 |
| 69.75139 | SiO₂ | -222 | Quartz, Tridymite, Cristobalite | 9.981 | 0.0001 | 0.523 |

The obtained values of the lattice microstrain (ε) are generally very low, indicating minimal distortion or defects in the crystal lattice of the nanoparticles. Higher lattice microstrains are observed for peaks with larger crystallite sizes, suggesting some degree of strain due to the growth or preparation process. The values show significant enhancement over some reported literature values (Table 2). The interplanar distance was also calculated using the Bragg equation shown below (Kelle *et al.*, 32023)

$$d_{(\theta)} = \frac{n\lambda}{sin\theta} \tag{5}$$

$d_{(\theta)}$ values are also recorded in Table 2. The interplanar distance $(d_\theta)$ represents the distance between adjacent crystallographic planes within the nanoparticles. It varies depending on the specific crystallographic plane and phase, with values ranging from around 0.5 to 3 Å. However, the range observed in this study is 0.562 to 7.121 Å, Peaks corresponding to different crystallographic planes of the same phase (e.g., Quartz) exhibit variations in crystallite size and lattice

microstrain. Some peaks show significant lattice microstrain, possibly due to factors such as strain induced during synthesis, crystal defects, or side effects. The identified phases and their corresponding peaks can be compared with reference XRD patterns or databases to validate the phase assignments and further characterize the nanoparticles.

**Table 2: Crystallite size and lattice microstrain for some SiONPs produced from plant materials**

| Plant Material | Synthesis Method | $d_x$ (nm) | $\varepsilon$ | Reference |
|---|---|---|---|---|
| **Rice Husk** | Electrochemical etching | 24.61-31.00 | - | Daulay *et al.* (2022) |
| **Rice Husk** | Magnethermic reduction with KBr | 24.58 - 28.81 | - | Gea & Al-Sagheer (2022) |
| **Bamboo Leaves** | Laser ablation in liquid | 2-10 | - | Li *et al.* (2017) |
| **Bamboo Leaves** | Molten salt-mediated synthesis | 5-20 | 0.2-0.4 | Li *et al.* (2021) |
| **Sawdust** | Sol-gel with citric acid | 10-20 | - | Peng & Li (2010) |
| **Leaves (unspecified)** | High-temperature calcination | 30-50 | - | Zhu *et al.* (2013) |
| **Hemp Stems** | Ball milling with NaOH | 15-30 | - | Wei *et al.* (2018) |
| **Corn Stover** | Hydrothermal method with CTAB | 10-20 | 0.3-0.5 | Zhang *et al.* (2014) |
| **Eucalyptus Wood** | Microwave-assisted method | 15-25 | 0.1-0.2 | Xu *et al.* (2019) |

Generally, the XRD results provide valuable information about the structural properties of silicon oxide nanoparticles, including phase composition, crystallite size, lattice microstrain, and interplanar distance, which are essential for understanding their physical and chemical properties and their potential applications in various fields. XRD peaks due to contaminants were not feasible in the observed pattern but the closeness of the peaks especially above 2Theta = 45 ° suggest that some amorphous character may be inherent in the SiONPs (Odoemelam *et al.*, 2023)

### 3.2 X-Ray Fluorescence analysis

X-ray fluorescence can be regarded as a unique technique for quantifying the presence of metal oxides in materials such as SiONPs. Consequently, the oxide and other contents of the synthesized SiONPs were tested for their percentage content and the results obtained are shown in Table 3. The results show that $SiO_2$ is the primary component of the nanoparticles and constitutes the bulk of the material at 95.18%. the transition metal oxides included in the analysis are CU), Ni), CoO, $V_2O_5$, $Cr_2O_3$, $Fe_2O_3$ and MgO. Each of them constitutes less than 1% and a total of 2.02%. The presence of these metal oxides can be regarded as dopant to the $SiO_2$. Trace concentrations of CaO (0.91), MgO (0.08%) and ZnO (1.07%) were also observed at concentrations slightly higher than the transition metal oxide. These metals are inherent components of the orange peel. For example, Ayala *et al.* (2021) have reported trace concentrations of Al, Ca, Na, and Fe in

orange peel. However, the current results did not indicate the presence of sodium since almost all the sodium was removed by washing as NaCl. Observed concentrations of other elements were lower than some reported values indicating that some of them were also removed during the processing. In addition, BaO, $Ta_2O_5$, $TiO_2$, $Ag_2O$, $ZrO_2$ and $SnO_2$ were observed at very low or negligible concentrations, contributing 0.1%. The presence of these metal oxides in the SiONPs can have a positive or negative influence on the material's properties and hence their applications. Their presence can affect their reactivity, adsorption capacity and mechanical strength through alteration in crystallinity, density, porosity, and band gap of the SiONPs.

**Table 3: XRF profiling for the oxide composition of the SiONPs**

| Compound | %C |
|---|---|
| $SiO_2$ | 95.18 |
| $V_2O_5$ | 0.00 |
| $Cr_2O_3$ | 0.03 |
| $MnO$ | 0.32 |
| $Fe_2O_3$ | 0.43 |
| $CoO$ | 0.41 |
| $NiO$ | 0.22 |
| $CuO$ | 0.61 |
| $Nb_2O_3$ | 0.00 |
| $MoO_3$ | 0.00 |
| $WO_3$ | 0.00 |
| $CaO$ | 0.91 |
| $MgO$ | 0.80 |
| $BaO$ | 0.00 |
| $Ta_2O_5$ | 0. 00 |
| $TiO_2$ | 0.02 |
| $ZnO$ | 1.07 |
| $Ag_2O$ | 0.00 |
| $ZrO_2$ | 0.00 |
| $SnO_2$ | 0.00 |

The performance of the SiONPs as catalysts can be enhanced through the presence of some metal oxides. For example, the transition metal ions.

In addition, some metal oxides can improve the electrical and optical properties of the SiONPs by altering their conductivity, bandgap, dielectric constant and optical transparency which can further enhance their applications as sensors, electronic devices, and photonic devices

The incorporation of metal oxides can affect the stability and durability of silicon oxide materials. Some metal oxides may enhance the thermal stability, chemical resistance, and mechanical durability of silicon oxide materials, leading to improved performance and longevity in harsh environments or under extreme conditions. Metal oxides can be used for functionalization and surface modification of silicon oxide materials. By incorporating specific metal oxides onto the surface or within the structure of silicon oxide materials, it is possible to introduce desired functionalities such as hydrophobicity, hydrophilicity, biocompatibility, antimicrobial properties, or specific chemical reactivity.

Finally, results from the XRF analysis indicate that the silicon oxide nanoparticles are primarily composed of $SiO_2$, with trace amounts of transition metal oxides and additional metal oxides present as impurities or additives. The presence of these impurities should be taken into consideration when assessing the material's properties and suitability for specific applications. Further characterization techniques, such as X-ray diffraction (XRD) or transmission electron microscopy (TEM), may provide additional insights into the nanoparticle's structure, morphology, and purity.

### 3.3 Scanning electron microscopy analysis

The scanning electron micrograph of the SiONPs is shown in Fig. 2. The micrograph reveals the presence of small, spherical

particles or structures clustered together but the particles seem to vary slightly in size but maintain a generally uniform shape.
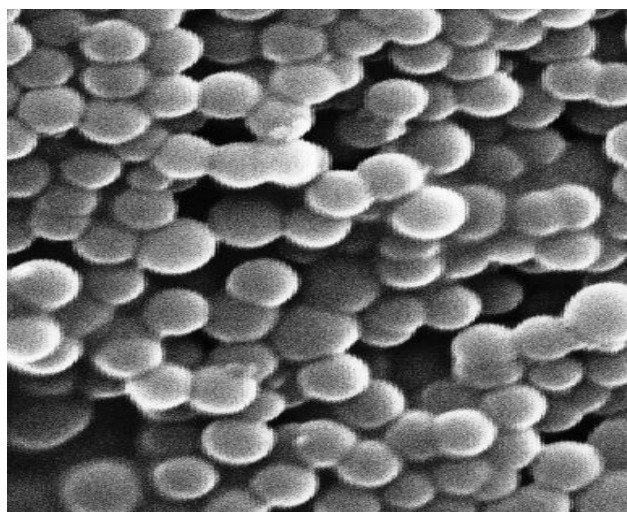


**Fig. 2: SEM Image of SiONPs obtained**

The scale bar indicates that the width of the image covers approximately 150 nanometers (nm). The image was taken at a magnification of 17000x. Based on the observed features, the image indicates that the SiONPs have some degree of orderly arrangement of the particles and depict higher level of crystallinity than amorphousness as observed from the phase separation of the XRD peaks in Fig. 1. The EDX profiling of the particles confirmed the

presence of Si (79%), O (18%), Ca (1.24%), $Al_2O_3$ (0.3%), C (0.04%), Mg (0.35), Zn (0.66%). The compositional analysis further confirmed that the produced nanoparticles are silicon oxide.

### 3.4    FTIR analysis

The FTIR spectrum of SiONPs obtained from orange peel is shown in Fig. 3. The spectrum was observed between frequencies of 400 and 3500 $cm^{-1}$ as a plot of percentage transmittance against wavenumber. The positions of the absorption peaks are recorded in Table 4.

The infrared (IR) spectrum represents the interaction of silicon oxide nanoparticles with infrared radiation. It provides information about the vibrational modes and functional groups present in the material. Fig. 4 reveals two significant observable peaks which were at 2500 and 2000 $cm^{-1}$. Around 2500 $cm^{-1}$: This peak corresponds to a specific vibrational mode associated with silicon oxide. The peak observed close to 2000 $cm^{-1}$ is another strong peak that is related to a different bond or structure within the nanoparticles. These two peaks generally confirm (between   2500 and 2000 $cm^{-1}$) specific chemical bonds or molecular vibrations in the silicon oxide nanoparticles.
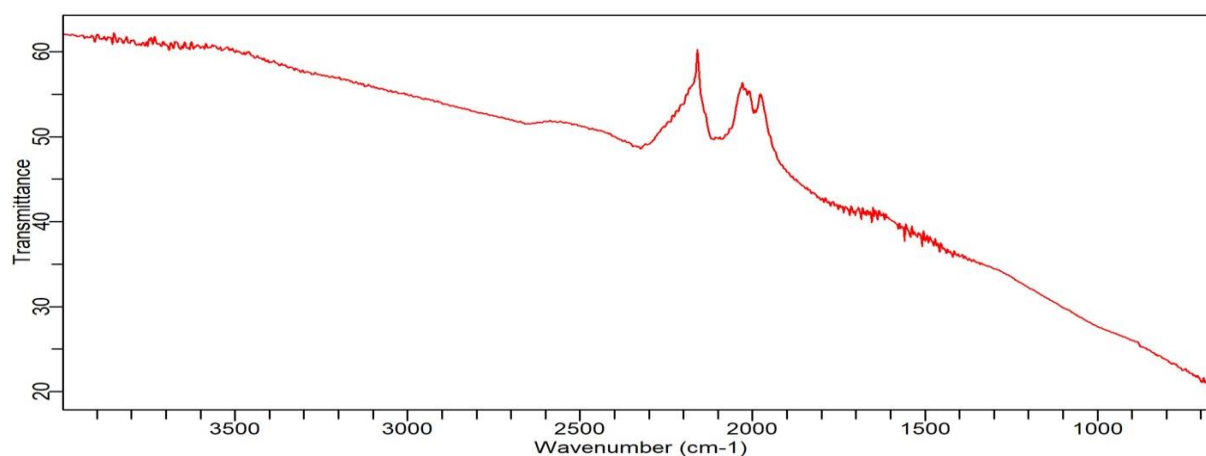


**Fig. 3: FTIR absorption spectrum of the SIONPs**

**Table 4.4: Infrared absorption data and assignment for the synthesized SiONPs**

| Peak Number | Wavenumber (cm$^{-1}$) | Assignment |
|:---:|:---:|:---|
| 1 | ~700 | Si-O-Si stretching vibrations |
| 2 | 1100-1200 | Si-O-Si asymmetric stretching vibrations |
| 3 | 1200-1300 | Si-O-Si symmetric stretching vibrations |
| 4 | 2000-2200 | Si-H stretching vibrations (common in hydrogen-terminated silicon nanoparticles) |
| 5 | 2100-2300 | Si-OH stretching vibrations (common in oxidized silicon nanoparticles) |
| 6 | 2350-2450 | Si-H stretching vibrations (common in hydrogen-terminated silicon nanoparticles) |

The assignments for the various absorption peaks are also shown in Table 4. The (i) Si-O-Si stretching vibrations are observed in the range of approximately 700 cm$^{-1}$ and are attributed to the stretching vibrations of silicon-oxygen-silicon bonds within the silicon oxide nanoparticles. Si-O-Si asymmetric and symmetric stretching vibrations are observed between 1100 and 1300 cm$^{-1}$ These peaks correspond to asymmetric and symmetric stretching vibrations of Si-O-Si bonds and confirms the structural integrity and composition of the silicon oxide nanoparticles. Peaks between 2000 and 2200 cm$^{-1}$, Si-H, are assigned to stretching vibrations of silicon-hydrogen (Si-H) bonds. These peaks are commonly observed in hydrogen-terminated silicon nanoparticles. Finally, peaks in the range of 2100-2300 cm$^{-1}$ are associated with stretching vibrations of silicon-hydroxyl (Si-OH) bonds. These peaks are indicative of surface oxidation in silicon nanoparticles.

### 4.5 Ultraviolet-Visible spectroscopic analysis

An absorption spectrum shows how a substance absorbs light at different wavelengths. The x-axis represents the wavelength (in nanometers, nm), and the y-axis represents the absorption intensity. The most significant feature in this spectrum is the peak around 420 nm. At this wavelength, the substance absorbs light most efficiently. The absorption value reaches approximately 1.93,

indicating strong absorption. Before and after the peak, the absorption values are relatively low (around 1.88). This baseline represents minimal absorption at those wavelengths.

The peak at 420 nm suggests that the substance interacts strongly with light in the visible region. This observation may be due to electronic transitions within the molecule (e.g., $\pi \rightarrow \pi^*$ or $n \rightarrow \pi^*$ transitions) or the presence of chromophores (light-absorbing groups) responsible for the absorption. The baseline absorption indicates that the substance does not significantly absorb light outside the peak region.
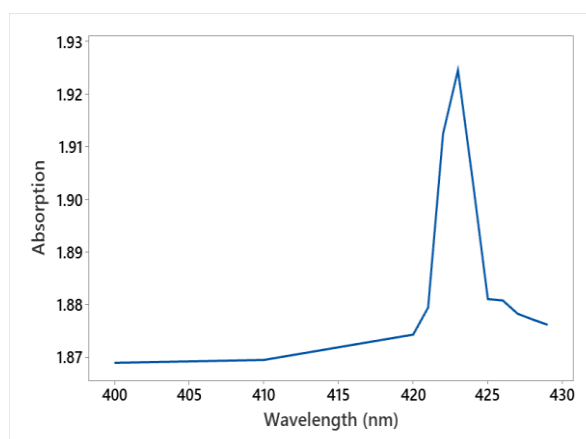


**Fig. 5: UV-Vis absorption spectrum of SiONPs**

UV-vis spectroscopy can provide information concerning the identification of the compound, quantitative analysis using Beer-Lambert law and in studying the electronic transitions in organic molecules.

The bandgap of the SiONPs can be calculated using the Planck equation given below (Eddy *et al*. 2023c-f)

$$E_{BG} = \frac{hc}{\lambda_{max}} \quad (6)$$

In equation 6, h represents the Planck constant, c is the speed of light and $\lambda_{max} = 420\ nm$ is the wavelength of maximum absorption by the SIONPs. Silicon oxide nanoparticles with a bandgap of approximately 2.91 eV can applied as photocatalysts for environmental remediation of organic contaminants. The silicon oxide nanoparticles can also be suitable as a UV filter with the capacity to block harmful UV light. This is particularly useful in sunscreen formulations, eyewear coatings, and protective films (Adimudo *et* al., 2023; Eddy *et al*., 2023g)

The materials can also be useful as fluorescent markers for imaging cells and tissues under UV light and targeted delivery of drugs or biomolecules. Also, incorporating silicon oxide nanoparticles can enhance solar cell efficiency because a tunable bandgap allows absorption across a broader spectrum. The materials can also be explored as anodes in lithium-ion batteries due to their high capacity.

## 4.0    Conclusion

This study investigates the feasibility of synthesizing silicon oxide nanoparticles (SiONPs) using orange peel waste as a precursor. The research aims to develop a sustainable and eco-friendly method for SiONP synthesis, exploring the presence of biomolecules in orange peel waste, optimizing synthesis processes, characterizing the synthesized nanoparticles, and exploring potential applications. By addressing these objectives, the study aims to contribute to sustainable nanotechnology practices and waste utilization. Further findings from the study included

(i)    Biomolecules in orange peel waste contain sufficient silicon to facilitate SiONP synthesis, making it a promising precursor for green synthesis methods.

(ii)    Optimized synthesis conditions, including reaction time, temperature, and concentration, enhance the efficiency of SiONP production from orange peel waste.

(iii)    Characterization techniques such as UV-Vis spectroscopy, XRD, and FTIR confirm the successful synthesis of SiONPs with desired properties, including size, shape, and composition.

(iv)    Preliminary functionalities of orange peel-derived SiONPs suggest potential applications in environmental remediation, drug delivery, and electronics.

(v)    The study fills a critical knowledge gap by being the first to directly utilize orange peel waste for SiONP synthesis, demonstrating the feasibility and potential of waste-to-nanoparticle approaches.

Therefore the study concludes that orange peel waste presents a viable and sustainable precursor for SiONP synthesis, offering numerous environmental and economic benefits. By developing a green synthesis method and exploring the unique properties of orange peel-derived SiONPs, the study contributes to advancing sustainable nanotechnology practices. The successful synthesis and characterization of SiONPs from orange peel waste underscore the potential of waste utilization in nanoparticle production, paving the way for greener and more efficient nanomaterial synthesis approaches.

Based on the findings, the study recommends further research to:

(i) Explore the scalability of the synthesis method for large-scale SiONP production.

(ii) Investigate the long-term stability and potential degradation of orange peel-derived SiONPs.

(iii) Conduct in-depth studies to fully explore and optimize potential applications of SiONPs in various fields.

(iv) Expand the scope to include other citrus fruit peels or plant waste for nanoparticle synthesis, broadening the applicability of waste-to-nanoparticle approaches.

(v) Collaborate with industries and policymakers to implement and commercialize sustainable nanoparticle synthesis methods using waste materials.

## 5.0    References

Adimudo, H. C., Agu, C. J., Okenyeka, O. U., Eddy, N. O., Dim, E. N., Dege, N., Bonardd, S., Vanka, K., Ibezim, A., Idika, D. I., Díaz, D. D., Obasi, N. L. (2023). Synthesis, characterization, crystal structure, in silico and computational studies on a novel Schiffbase derived from α-chlorocinnamaldehyde and 4-aminoantipyrine, Journal of Molecular Structure, https://doi.org/10.1016/j.molstruc.2023.135928. (Thompson Reuters (TR) Impact Factor = 3.841)

Amanulla, A. M., & Sundaram, R. (2019). Green synthesis of $TiO_2$ nanoparticles using orange peel extract for antibacterial, cytotoxicity and humidity sensor applications. *Materials Today: Proceedings*, 8 (1): 323-331. ISSN 2214-7853. https://doi.org/10.1016/j.matpr.2019.02.118.

Anjum, A., Garg, R., Kashif, M. and Eddy, N. O. (2023). Nano-scale innovations in packaging: properties, types, and applications of nanomaterials for the future. *Food Chemistry Advances,* 100560, https://doi.org/10.1016/j.focha.2023.100560.

Bashir, M., Ali, S., & Farrukh, M. A. (2020). Green Synthesis of $Fe_2O_3$ nanoparticles from orange peel extract and a study of its antibacterial activity. *Journal of the Korean Physical Society*, 76, 848–854. https://doi.org/10.3938/jkps.76.848.

Bishnoi, S., Kumar, S., & Chandra, S. (2018). A review on the applications of green synthesized nanoparticles. *Critical Reviews in Environmental Science and Technology*, 48(1), 68-125.

Dang-Bao, T., Ho, T. G.-T., Do, B. L., Anh, N. P., Phan, T. D. T., Tran, T. B. Y., Duong, N. L., Phuong, P. H., & Nguyen, T. (2022). Green Orange Peel-Mediated Bioinspired Synthesis of Nanoselenium and Its Antibacterial Activity against Methicillin-Resistant Staphylococcus aureus. *ACS Omega*, 7(40), 36037-36046. https://doi.org/10.1021/acsomega.2c05469.

Doan Thi, T. U., Nguyen, T. T., Thi, Y. D., Ta Thi, K. H., Phan, B. T., & Pham, K. N. (2020). Green synthesis of ZnO nanoparticles using orange fruit peel extract for antibacterial activities. *RSC Advances*, 10(40), 23899-23907. https://doi.org/10.1039/D0RA04926C.

Eddy, N. O., Edet, U. E., Oladele J. O., Kelle, H. I., Ogoko. E. C., Odiongenyi, A. O., Ameh, P., Ukpe, R. A., Ogbodo, R., Garg, R. & Garg, R. (2023g). Synthesis and application of novel microporous framework of nanocomposite from trona for photocatalysed degradation of methyl orange dye. *Environmental Monitoring and Assessment*. DOI : 10.1007/s10661-023-12014-x,

Eddy, N. O., Garg, R., Garg, R., Eze, S. I., Ogoko, E. C., Kelle, H. I., Ukpe, R. A., Ogbodo, R. & Chijoke, F. (2023a). Sol-gel synthesis, computational chemistry, and applications of CaO nanoparticles for the remediation of methyl orange contaminated water. Advances in Nano Research,

https://doi.org/10.12989/anr.2023.15.1.000.

Eddy, N. O., Garg, R., Garg, R., Garg, R., Ukpe, R. A. & Abugu, H. (2024c). Adsorption and photodegradation of organic contaminants by silver nanoparticles: isotherms, kinetics, and computational analysis. *Environ Monit Assess,* 196, 65, https://doi.org/10.1007/s10661-023-12194-6. Impact Factor = 3.201. Q2 Journal. Published by Springer Nature.

Eddy, N. O., Garg, R., Garg, R., Ukpe, R. A. & Abugu, H. (2023f). Adsorption and photodegradation of organic contaminants by silver nanoparticles: isotherms, kinetics, and computational analysis. *Environmental Monitoring and Assessment,,* DOI : 10.1007/s10661-023-12194-6,

Eddy, N. O., Garg, R., Ukpe, R. A., Ameh, P. O., Gar, R., Musa, R., , Kwanchi, D., Wabaidur, S. M., Afta, S., Ogbodo, R., Aikoye, A. O., & Siddiqu, M. (2024b). Application of periwinkle shell for the synthesis of calcium oxide nanoparticles and in the remediation of $Pb^{2+}$-contaminated water. *Biomass Conversion and Biorefinery*, DOI: 10.1007/s13399-024-05285-y.

Eddy, N. O., Jibrin, J. I., Ukpe, R. A., Odiongenyi, A. O., Kasiemobi, A. M., Oladele, J. O. and Runde, M. (2024a). Experimental and Theoretical Investigations of Photolytic and Photocatalysed Degradations of Crystal Violet Dye (CVD) in Water by oyster shells derived CaO nanoparticles (CaO-NP), *Journal of Hazardous Materials Advances,* 100413, https://doi.org/10.1016/j.hazadv.2024.100413.

Eddy, N. O., Odiongenyi, A. O., Garg, R., Ukpe, R. A., Garg, R., El Nemir, A., Ngwu, C. M. and Okop, I. J. (2023c).

Quantum and experimental investigation of the application of *Crassostrea gasar* (mangrove oyster) shell–based CaO nanoparticles as adsorbent and photocatalyst for the removal of procaine penicillin from aqueous solution. *Environmental Science and Pollution Research*, doi:10.1007/s11356-023-26868-8.

Eddy, N. O., Ukpe, R. A., Ameh, P., Ogbodo, R., Garg, R. and Garg, R. (2023i). Theoretical and experimental studies on photocatalytic removal of methylene blue (MetB) from aqueous solution using oyster shell synthesized CaO nanoparticles (CaONP-O). Environmental Science and Pollution Research, https://doi.org/10.1007/s11356-022-22747-w.

Eddy, N. O., Ukpe, R. A., Garg, R., Garg, R., Odiongenyi, A. O., Ameh, P., Akpet, I, N., and Udo, E. S. (2023d). Review of in-depth knowledge on the application of oxides nanoparticles and nanocomposites of Al, Si and Ca as photocatalyst and antimicrobial agents in the treatment of contaminants in water. Clean Technologies and Environmental Policy, DOI : 10.1007/s10098-023-02603-2.

Epstein, E. (1999). Silicon. Annual Review of Plant Physiology and Plant Molecular Biology, 50(1), 641-664.

Garg, R. Rani, P., Garg, R. and Eddy, N. O. (2021). Study on potential applications and toxicity analysis of green synthesized nanoparticles. *Turkish Journal of Chemistry*, 45, doi:10.39906/kim-2106-59.

Garg, R., Garg, R. and Eddy, N. O. (2024da). Chapter 4: Applications of nocomposites in Water Remediation: A Mechanistic Overview, doi: 10.4018/979-8-3693-1094-6.ch004. Pp. 102-120

Garg, R., Garg, R., Eddy, N. O., Almohana, A. I., Fahad, S., Khan, M. A. and Hong, S. H.

(2022). Biosynthesized silica-based zinc oxide nanocomposites for the sequestration of heavy metal ions from aqueous solutions. *Journal of King Saud University*-Science https://doi.org/10.1016/j.jksus.2022.101996..

Garg, R., Mittal, M., Tripathi, S., & Eddy, N. O. (2024b). Core to concept: synthesis, structure, and reactivity of nanoscale zero-valent iron (NZVI) for wastewater remediation. *Environmental Science and Pollution Research*. Advance online publication. https://doi.org/10.1007/s11356-024-33197-x

Gea, S., & Al-Sagheer, F. A. (2022). Synthesis Si nanoparticles from rice husk as material active electrode on secondary cell battery with X-Ray Diffraction Analysis. South African Journal of Chemical Engineering, 42, 32–41.

Kazemi, S., Hosseingholian, A., Gohari, S. D., Feirahi, F., Moammeri, F., Mesbahian, G., Moghaddam, Z. S., & Ren, Q. (2023). Recent advances in green synthesized nanoparticles: from production to application. *Materials Today Sustainability*, 24, 100500. https://doi.org/10.1016/j.mtsust.2023.100500.

Kelle, H. I., Ogoko, E. C., Akintola O and Eddy, N. O. (2023b). Quantum and experimental studies on the adsorption efficiency of oyster shell–based CaO nanoparticles (CaONPO) towards the removal of methylene blue dye (MBD) from aqueous solution. Journal: Biomass Conversion and Biorefinery, DOI : 10.1007/s13399-023-04947-7.,

Khan, I., Khan, T., & Khan, S. (2021). Applications of green synthesized nanoparticles in sustainable agriculture. *Sustainable Agriculture Reviews*, 64, 187-221.

More, A. S., Patil, D. D., & Bhosale, B. V. (2023). Plant extract mediated synthesis of silver nanoparticles and their application in textile dyeing. *Materials Today Proceedings*, 62, 1252-1258.

Odoemelam, S. A., Oji, E. O., Eddy, N. O., Garg, R., Garg, R., Islam, S., Khan, M. A., Khan, N. A. and Zahmatkesh, S. (2023e). Zinc oxide nanoparticles adsorb emerging pollutants (glyphosate pesticide) from aqueous solution. *Environmental Monitoring and Assessment*, https://doi.org/10.1007/s10661-023-11255-0.

Omran, A. A. (2020). Green synthesis and applications of metallic nanoparticles. *Artificial Cells, Nanomedicine, and Biotechnology*, 48(1), 323-334.

Rashwan, E. A., Abdelhameed, R. H., Fouda, A., & Mohd Yusoff, M. I. (2022a). Synthesis of green nanoparticles for energy, biomedical, environmental, agricultural, and food applications: A review. *Journal of Materials Science*, 57(29):14805-14848.

Salem, S. S., Badawy, M. S. E. M., Al-Askar, A. A., Arishi, A. A., Elkady, F. M., & Hashem, A. H. (2022). Green Biosynthesis of Selenium Nanoparticles Using Orange Peel Waste: Characterization, Antibacterial and Antibiofilm Activities against Multidrug-Resistant Bacteria. *Life (Basel)*, 12(6), 893. https://doi.org/10.3390/life12060893.

Tavker, M. A., Soliman, D. A., & Abdelhameed, R. H. (2021). Recent trends in the green synthesis of metallic nanoparticles using plant extracts. *Bioengineering*, 8(10), 142.

Xu, Y., Zhu, C., Liu, Y., Luo, S., & Li, C. (2019). A facile microwave-assisted synthesis of silicon nanoparticles from eucalyptus wood for high-performance lithium-ion battery anodes. Journal of Alloys and Compounds, 780, 101-108.

Ying, S., Guan, Z., Ofoegbu, P. C., Clubb, P., Rico, C., He, F., & Hong, J. (2022). Green synthesis of nanoparticles: Current developments and limitations. *Environmental Technology & Innovation*, 26, 102336. https://doi.org/10.1016/j.eti.2022.102336.

**Compliance with Ethical Standards**

**Declarations**:
The authors declare that they have no conflict of interest.
**Data availability**: All data used in this study will be readily available to the public.
**Consent for publication**: Not Applicable.

**Availability of data and materials**: The publisher has the right to make the data public.
**Competing interests**
 The authors declared no conflict of interest.

**Authors' Contributions**
Heleen carried out the laboratory experiment. Richard design the work and wrote the manuscript. Both authors were involved in the correction of the manuscript